JOURNAL OF GUIDANCE, CONTROL, AND DYNAMICS
Vol. 19, No. 1, January–February 1996

Nonlinear Trajectory Tracking Guidance with Application to a Launch Vehicle

Ping Lu*
Iowa State University, Ames, Iowa 50011-3231

This paper presents a methodology for nonlinear guidance law design for aerospace vehicles to track a prescribed nominal trajectory. The guidance law is based on a continuous-time predictive control concept and is applicable to vehicles with general nonlinear dynamics. The feedback guidance commands can be obtained reliably and efficiently by a convergent fixed-point algorithm. A launch vehicle trajectory-tracking problem is used to demonstrate the application. Asymptotic tracking convergence under the proposed method is studied analytically. The guidance law guarantees the satisfaction of the angle-of-attack constraint and a normal load constraint. Simulations are done to test the guidance law for a variety of trajectory dispersions, disturbances, and modeling uncertainties.

I. Introduction

THE trajectory-tracking problem discussed in this paper is specifically defined as follows: given the dynamic model of an aerospace vehicle that is often nonlinear, and a nominal trajectory that satisfies all of the mission requirements and constraints, determine the control commands that would guide the vehicle to track the nominal trajectory in the presence of trajectory dispersions and external disturbances. An apparent approach is to use linear control techniques, such as linear quadratic regulator (LQR) and pole placement, applied to the linearized system. Since the linearized dynamics are generally time varying, the feedback gains will be time varying, and so either gain scheduling or piecewise-constant gains will have to be used instead.[1] The small perturbation assumption required for the validity of linearization can also be a restricting factor.

An effective existing approach for nonlinear tracking control is based on the so-called geometric control theory.[2] This approach involves a nonlinear coordinate transformation and static state feedback to transform the nonlinear system into a linear, controllable system and is known as dynamic inversion in the aerospace control community.[3–5] The geometric control approach is used in Refs. 6 and 7 to obtain control laws to track near-optimal ascent trajectories for an aerospace plane. In some aerospace guidance problems, however, the variables chosen to be the controls do not appear linearly in the dynamic equations, and constraints on controls and trajectory are always present. In these cases, this approach is not always convenient to use.

A predictor-corrector guidance algorithm is used in Ref. 8 for an aerospace plane to track the optimal ascent trajectory. Some heuristic schemes for particular applications have also been proposed that are derived on the basis of some characteristics of the trajectory and dynamics.[9,10] Although they can be effective if appropriately designed, there are no systematic guidelines as to how one should proceed to derive them, and there is a lack of underlying theory.

It is the intent of this paper to examine aerospace trajectory-tracking guidance problems from a different perspective. A systematic methodology for guidance law design is introduced that is applicable to aerospace vehicles with general nonlinear dynamics. The approach is based on a recently developed continuous predictive control concept[11,12] that also handles control saturations explicitly. A launch vehicle trajectory tracking problem is solved to gain some insight and demonstrate the features of this method. The rest of the paper is divided into four sections. Section II reviews briefly the nonlinear predictive control method that obtains a feedback control law based on minimization of the difference between the predicted and desired responses. An asymptotic tracking property of the control law is presented in Sec. III for a class of systems that are linear in the control. In Sec. IV the technique is applied to the trajectory-tracking problem for a generic heavy-lift launch vehicle to follow a predesigned minimum-fuel trajectory. Asymptotic tracking convergence and a method to enforce an inequality trajectory constraint for the launch vehicle are discussed. Trajectory-tracking performance of the guidance law for a variety of off-nominal perturbations and disturbances are examined. Section V summarizes the work.

Received Feb. 23, 1994; revision received July 14, 1994; accepted for publication June 10, 1995.

*Associate Professor, Department of Aerospace Engineering and Engineering Mechanics, 304 Town Engineering Building. Senior Member AIAA.

II. Nonlinear Continuous-Time Predictive Control Laws

The following is a brief review of the continuous predictive control method to be used. The reader is referred to Refs. 11 and 12 for more complete development.

Prediction of System Response

Consider a nonlinear dynamic system of the general form

$$\dot{x}_1 = f_1(x) \tag{1}$$

$$\dot{x}_2 = f_2(x) + g_2(x, u) \tag{2}$$

where $x_1 \in \boldsymbol{R}^{n_1}$, $x_2 \in \boldsymbol{R}^{n_2}$ with $n_1 \geq 0$, $n_2 > 0$, and $n_1 + n_2 = n$; $x = (x_1^T \; x_2^T)^T \in \boldsymbol{R}^n$ is the state vector, and $u(t) \in \boldsymbol{U} = \{u(t) \in \boldsymbol{R}^m \mid L_i[x(t)] \leq u_i(t) \leq U_i[x(t)]\}$ is the control vector, where the bounds L_i and U_i are specified and allowed to be state dependent. The f_1: $\boldsymbol{R}^n \to \boldsymbol{R}^{n_1}$, f_2: $\boldsymbol{R}^n \to \boldsymbol{R}^{n_2}$, and g_2: $\boldsymbol{R}^n \times \boldsymbol{R}^m \to \boldsymbol{R}^{n_2}$ are continuously differentiable nonlinear functions. Equation (1) typically represents the kinematics and Eq. (2) the dynamics of the system. Suppose that a desired trajectory $x^*(t) \in \boldsymbol{R}^n$, $t \in [0, t_f]$, is already known. An important assumption we need is the feasibility of the desired trajectory.

The desired trajectory $x^*(t)$ satisfies the system Eqs. (1) and (2) with a corresponding control $r^*(t) \in \boldsymbol{U}$.

This assumption assures that the nominal trajectory is achievable, which is usually the case in aerospace applications where $x^*(t)$ often is either a carefully planned trajectory or an optimal trajectory obtained off line based on the system model. The explicit knowledge of $r^*(t)$ is not necessary when the system is linear in u, as will be seen, but it is required when the system is nonlinear in u. Note that although only full-state tracking is discussed in the following, it is straightforward to apply the same approach to partial-state tracking or output tracking.

Suppose that the second-order derivative of each component of x_1 contains components of u explicitly, and the first-order derivative of each component of x_2 depends on components of u explicitly. More general situations can be handled in a similar way, but this usually

suffices for aerospace trajectory-tracking guidance problems. If at an arbitrary instant $t \in [0, t_f]$, $x(t)$ is known, then the current control $u(t)$ determines the system response in the immediate future. Specifically, consider the response $x(t+h)$, where $h > 0$ is a small time increment. Since $\ddot{x}_1(t)$ and $\dot{x}_2(t)$ depend on $u(t)$ explicitly, we may predict the influence of $u(t)$ on $x_1(t+h)$ by a second-order Taylor series expansion at t and on $x_2(t+h)$ by a first-order expansion:

$$x_1(t+h) \approx x_1(t) + hf_1[x(t)] + (h^2/2)\{F_{11}[x(t)]f_1[x(t)] + F_{12}[x(t)]f_2[x(t)] + F_{12}[x(t)]g_2[x(t), u(t)]\} \tag{3}$$

$$x_2(t+h) \approx x_2(t) + h\{f_2[x(t)] + g_2[x(t), u(t)]\} \tag{4}$$

where $F_{11} = \partial f_1[x(t)]/\partial x_1$ and $F_{12} = \partial f_1[x(t)]/\partial x_2$ (the derivative of each component of f_1 with respect to x is defined as a row vector). Also, partition $x^*(t)$ accordingly into $[x_1^{*T}(t)\ \ x_2^{*T}(t)]^T$, and expand $x_1^*(t+h)$ and $x_2^*(t+h)$ in similar ways:

$$x_1^*(t+h) \approx x_1^*(t) + h\dot{x}_1^*(t) + (h^2/2)\ddot{x}_1^* \tag{5}$$

$$x_2^*(t+h) \approx x_2^*(t) + h\dot{x}_2^* \tag{6}$$

The tracking error at $t+h$ can then be approximated by

$$e_1(t+h) = x_1(t+h) - x_1^*(t+h) \approx e_1(t) + h\dot{e}_1(t) + 0.5h^2\left[F_{11}(x)f_1(x) + F_{12}(x)f_2(x) + F_{12}(x)g_2(x,u) - \ddot{x}_1^*\right] \tag{7}$$

$$e_2(t+h) = x_2(t+h) - x_2^*(t+h) \approx e_2(t) + h\left[f_2(x) + g_2(x,u) - \dot{x}_2^*\right] \tag{8}$$

where the dependence of $x(t)$, $x^*(t)$, and $u(t)$ on t in the right-hand sides of the Eqs. (7) and (8) has been suppressed for simplicity.

Continuous Predictive Control Law

To determine the control $u(t)$ so as to reduce the tracking errors, let us consider the minimization of the following performance index:

$$\min_{u(t)\in U} J = \tfrac{1}{2}e_1^T(t+h)Q_1(t)e_1(t+h) + \tfrac{1}{2}e_2^T(t+h)Q_2(t)e_2(t+h) + \tfrac{1}{2}[u(t) - r^*(t)]^T R(t)[u(t) - r^*(t)] \tag{9}$$

where Q_1 and Q_2 are positive semidefinite matrices and R positive definite, all with appropriate dimensions and possibly time dependent if needed. Replacing $e_1(t+h)$ and $e_2(t+h)$ by Eqs. (7) and (8), we have a parameter optimization problem with respect to $u(t)$ defined by Eq. (9). When the optimal solution to problem (9) lies in the interior of the control set U, the necessary condition for optimality is $\partial J/\partial u = 0$, which leads to

$$u(t) = r^*(t) - hR^{-1}\left(0.5h\left[F_{12}(x)\frac{\partial g_2(x,u)}{\partial u}\right]^T \times Q_1\left\{e_1 + h\dot{e}_1 + 0.5h^2\left[F_{11}(x)f_1(x) + F_{12}(x)f_2(x) + F_{12}(x)g_2(x,u) - \ddot{x}_1^*\right]\right\} + \left[\frac{\partial g_2(x,u)}{\partial u}\right]^T \times Q_2\left\{e_2(t) + h\left[f_2(x) + g_2(x,u) - \dot{x}_2^*\right]\right\}\right) \triangleq \eta(u) \tag{10}$$

where for a given h the mapping η: $\boldsymbol{R}^m \to \boldsymbol{R}^m$ is defined for u, since all other quantities are either known or specified (Q_1, Q_2, and R). Because $t \in [0, t_f]$ is arbitrary, Eq. (10) defines a continuous, implicit control law for u, with a feedforward term r^* and a feedback part associated with the tracking errors. When the system is linear in u, that is, $g_2(x,u) = B_2(x)u$, a closed-form solution for u can be obtained from Eq. (10),

$$u(t) = -P^{-1}\left\{(h^2/2)(F_{12}B_2)^T Q_1\left[e_1 + h\dot{e}_1 + (h^2/2)\left(F_{11}f_1 + F_{12}f_2 - \ddot{x}_1^*\right)\right] + hB_2^T Q_2\left[e_2 + h\left(f_2 - \dot{x}_2^*\right)\right] - Rr^*\right\} \tag{11}$$

where

$$P = \left[0.25h^4(F_{12}B_2)^T Q_1 F_{12}B_2 + h^2 B_2^T Q_2 B_2 + R\right] \tag{12}$$

It is clear in this case that R can be set to zero as long as P is still nonsingular, and hence the dependence of u on r^* can be eliminated. When the system equations (2) are nonlinear in u, there is no analytical solution for u from Eq. (10) in general. Numerical algorithms must be employed to solve for u. Difficulties that may be encountered include that multiple solutions to Eq. (10) may exist, some of which are merely stationary points rather than minimizing solutions; the convergence of the algorithm cannot be guaranteed for all of the points along the trajectory; the computation required may be too excessive for on-line implementation. All of these questions must be answered satisfactorily if the technique is to have potential practical use. Let us introduce a vector saturation function s: $\boldsymbol{R}^m \to \boldsymbol{U}$ to handle the bounds on the control. For any $y \in \boldsymbol{R}^m$ the ith component of $s(y)$ ($1 \le i \le m$) is defined as

$$s_i(y) = \begin{cases} U_i, & y_i \ge U_i \\ y_i, & L_i < y_i < U_i \\ L_i, & y_i \le L_i \end{cases} \tag{13}$$

We have the following results regarding the preceding questions.

Theorem 1. At any $t \in [0, t_f]$, for any given bounded values of $x(t)$, $x^*(t)$, $r^*(t)$, $Q_1 \ge 0$, $Q_2 \ge 0$, and $R > 0$, there always exists a sufficiently small $h_0 > 0$ such that for all $0 < h \le h_0$ the implicit equation in u

$$u = s[\eta(u)] \tag{14}$$

has a unique solution $u^* \in \boldsymbol{U}$. When u^* is in the interior of $\boldsymbol{U}$, it is the unique optimal solution of the problem (9). Furthermore, define a ball $B_\delta = \{u \in \boldsymbol{R}^m \mid \|u - r^*\| \le \delta\}$ for some $\delta > 0$. Then, the fixed-point iteration sequence $\{u^k\}$ generated by

$$u^k = s[\eta(u^{k-1})], \qquad k = 1, 2, \ldots, \qquad \forall u^0 \in B_\delta \tag{15}$$

converges to u^*.

The proof of the Theorem, given in Ref. 11, is based on the argument that the mapping $u = s[\eta(u)]$ is a local contraction mapping in B_δ for sufficiently small h.

Remarks

1) We note that Eq. (14) is the same as Eq. (10) when $\eta(u) \in \boldsymbol{U}$. Equation (14) provides an implicit feedback control law to the tracking problem. The pointwise-optimal control u^* can be conveniently obtained by the fixed-point iteration (15) that is guaranteed to converge for sufficiently small h. Fixed-point iteration is particularly suited for digital computer implementation. If we rewrite the control law (14) as

$$u = s[r^* - hR^{-1}N(x, x^*, u)] \tag{16}$$

where the nonlinear vector term N is obviously defined by comparing the argument of $s[\cdot]$ with the expression of $\eta(u)$ in Eq. (10), a schematic diagram for continuous-time implementation of the control law is shown in Fig. 1.

2) On the basis of the assumption that $x^*(t)$ and $r^*(t)$ satisfy the system model Eqs. (1) and (2), one can easily verify that when $e(t_0) = 0$ at any $t_0 \in [0, t_f]$, $u(t_0) = r^*(t_0)$ makes J in Eq. (9) vanish for any $h > 0$. This indicates that a solution of the optimization problem (9) in this case is exactly $r^*(t_0)$ (because $J \ge 0$ for any u), and by Theorem 1 the iteration (15) will converge to $r^*(t_0)$ for sufficiently small h. It thus follows that the tracking error $e(t)$ will remain zero for $t_0 \le t \le t_f$.

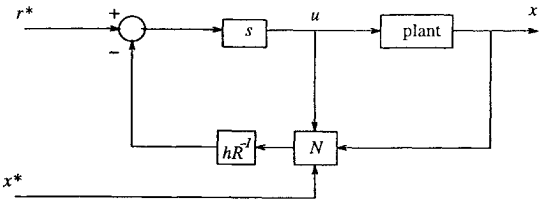

Fig. 1 Continuous-time implementation of the control law.

3) The prediction horizon h need not be as small as the "integration step size," even though truncated Taylor series expansions are used in the derivation (see Sec. III). In fact, it can be treated as a controller parameter that can be tuned for better tracking performance. It should be noted, however, that a value of h that is small enough for the fixed-point iteration (15) to converge at one point may not be sufficiently small at another point along the trajectory. For a given problem it is usually not difficult to find through numerical simulations a value of h that will work for all of the points on the entire trajectory. However, we stress that it is not advisable to choose a very small h for this purpose, because too small an h tends to diminish the effectiveness of the control. This can be seen from Eq. (10): when $h \approx 0$, $u(t) \approx r^*(t)$, regardless of the sizes of the tracking errors $e_1(t)$ and $e_2(t)$. Therefore, it may work better for some more demanding problems, as will be seen in Sec. IV, if a simple adaptive scheme is included that always starts with a given moderate h and will reduce the size of h if convergence has not been achieved at a point after a specified number of iterations. Convergence will occur typically within only a few iterations if h is adequately small.

4) Finally, since this approach allows the constraints of the controls to be state dependent, the control law can reinforce both inequality control constraints and trajectory constraints conveniently by selecting the U_i and L_i in Eq. (13) appropriately. Such an application is demonstrated in Sec. IV. More general development and discussion will be given in a forthcoming paper.

III. Asymptotic Tracking Property

Although the control law is derived based on minimization of local tracking errors, global asymptotic tracking convergence can be proven for several classes of systems that are linear in controls. Let us consider the following system that will be used in the next section:

$$\dot{x}_1 = Ax_2 \tag{17}$$

$$\dot{x}_2 = f_2(x) + B_2(x)u \tag{18}$$

Assume that $n_1 \leq n_2 = m$, the constant matrix A has a rank of n_1, and $\text{rank}(B_2(x)) = m$, where, as in Sec. II, $n_1 = \dim(x_1)$, $n_2 = \dim(x_2)$, $n = n_1 + n_2$, and $m = \dim(u)$. Note that the dimensions of x_1 and x_2 are not required to be the same. Suppose that a reference trajectory $x^* = (x_1^* \; x_2^*)$ is given where according to the feasibility assumption x_1^* and x_2^* satisfy $\dot{x}_1^* = Ax_2^*$. We have the following global asymptotic tracking property.

Theorem 2. For any $Q_1 > 0$, $Q_2 > 0$, and $h > 0$, control law (11) guarantees, in the absence of control saturation, globally asymptotically stable tracking of the reference trajectory $x^*(t)$ for system (17) and (18) when the weighting $R \to 0$.

Proof: Letting $R = 0$ in the control law (11) and applying it to system (17) and (18) give

$$u(t) = -B_2^{-1}P\Big(\tfrac{1}{2}A^TQ_1\big\{e_1 + h\dot{e}_1 + (h^2/2)\big[Af_2 - \ddot{x}_1^*(t)\big]\big\} + (1/h)Q_2\big\{e_2 + h\big[f_2 - \dot{x}_2^*(t)\big]\big\}\Big) \tag{19}$$

where

$$P = \big(0.25h^2A^TQ_1A + Q_2\big)^{-1} > 0 \tag{20}$$

Substitute Eq. (19) into the system equations (17) and (18). The tracking error dynamics are

$$\dot{e}_1 = Ae_2 \tag{21}$$

$$\dot{e}_2 = -\tfrac{1}{2}PA^TQ_1e_1 - (1/h)P\big(\tfrac{1}{2}h^2A^TQ_1A + Q_2\big)e_2 \tag{22}$$

To study the stability of Eqs. (21) and (22), we consider a Lyapunov function candidate

$$V = \tfrac{1}{4}e_1^TQ_1e_1 + \tfrac{1}{2}e_2^TP^{-1}e_2 > 0, \quad \text{for all } e = \big(e_1^T \; e_2^T\big)^T \neq 0 \tag{23}$$

Thus,

$$\dot{V} = -e_2^T\big[(h/2)A^TQ_1A + (Q_2/h)\big]e_2 \leq 0 \quad \text{for all } e \tag{24}$$

By LaSalle's invariant theorem[13] the solution $e(t)$ of Eqs. (21) and (22) tends to the invariant set

$$S = \big\{e \in R^n \mid e_2 = 0,\ PA^TQ_1e_1 = 0\big\} \tag{25}$$

Since P and Q_1 are nonsingular and $n_1 \leq n_2$, the $n_2 \times n_1$ matrix PA^TQ_1 has a rank of n_1 if $\text{rank}(A) = n_1$. It thus follows that $PA^TQ_1e_1 = 0 \Rightarrow e_1 = 0$. Therefore, $S = \{0\}$. So $e = 0$ is globally asymptotically stable.

Note that in this case the asymptotic tracking convergence holds for any $h > 0$ that is not necessarily small. This result is somewhat surprising at first, given that Taylor series expansions are used in predicting the system response, but it has a logical explanation after we look at the approach closely. In this predictive control setting, the signs of the higher order terms in the Taylor series expansions are more important than their accuracy.

For systems that are also nonlinear in controls, a direct general proof of asymptotic stability under the implicit control law (14) is not available. But if a redefinition of control inputs can be used to transform such a system into a form that is linear in control, and the transformed system is asymptotically stable under the corresponding predictive controller (11), the validity of the control approach may be established indirectly by observing that both control laws (11) and (14) minimize the same performance index (9) as $R \to 0$. In the next section such an example is provided.

IV. Trajectory Tracking for a Launch Vehicle

In this section the preceding approach is applied in simulations to track a nominal trajectory for a heavy-lift launch vehicle. The current launch vehicles are typically guided by preprogrammed open-loop pitch and yaw profiles for the atmospheric portion of ascent and then by linear tangent steering law for the vacuum portion of flight.[14–16] Some recent studies[17,18] examine the use of regular perturbation techniques for possible in-flight generation of near-optimal trajectories. In the approach proposed here, there are two aspects: generating a nominal trajectory off line and tracking the nominal trajectory on line, and this paper concerns the latter. The nominal ascent trajectory used in this section is generated off line as the result of a trajectory optimization problem. (The optimality of the trajectory is not required in the current approach, though. The nominal trajectory can be any feasible trajectory.) The feedback guidance laws based on the predictive control technique are employed to track the nominal trajectory.

Vehicle Model and Optimal Ascent Trajectory

An advanced launch system model provided by NASA Langley Research Center is used here (which is the same one used in Refs. 10, 17, and 18). The system consists of a liquid rocket booster and a core vehicle as shown in Fig. 2. The booster has seven rocket engines, each producing a vacuum thrust of 2,580,457 N. The core vehicle has three identical engines. The vacuum specific impulse for the engines is $I_{sp} = 430$ s. Other parameters for the core vehicle are payload + fairing = 72,161 kg, inert mass = 79,891 kg, and maximum fuel mass = 678,669 kg. For the booster, the inert mass = 79,891 kg, and the maximum fuel mass = 679,930 kg. The payload is to be put into a 148.16 × 277.8 km (80 × 150 n mile) Earth orbit at perigee. The first stage of the vehicle is the combination of the

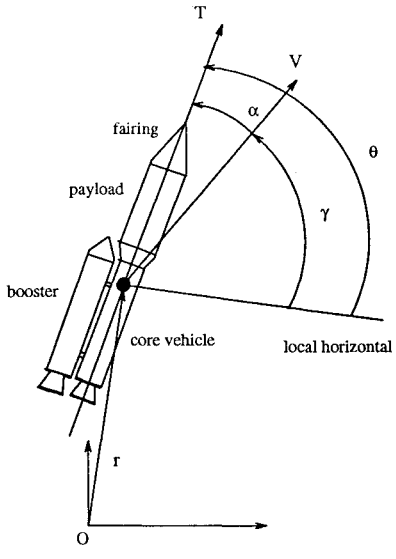

Fig. 2 Launch vehicle configuration.

booster and the core vehicle. All 10 engines are ignited at liftoff. The second stage refers to the core vehicle that continues the flight after the booster burns out and is jettisoned. The point-mass equations of motion of the vehicle in a vertical plane over a nonrotating, spherical Earth are

$$\begin{aligned} \dot{r} &= v\sin\gamma \\ \dot{v} &= \frac{T\cos(\theta-\gamma)-D}{m} - \frac{\mu\sin\gamma}{r^2} \\ \dot{\gamma} &= \frac{T\sin(\theta-\gamma)+L}{mv} + \left(\frac{v}{r} - \frac{\mu}{vr^2}\right)\cos\gamma \\ \dot{m} &= -\frac{T_0}{g_0 I_{sp}} \end{aligned} \tag{26}$$

where r is the radius from the center of the Earth to the vehicle, v the velocity, γ the flight-path angle, θ the pitch angle of the vehicle, m the mass, D the aerodynamic drag, L the lift, and μ the gravitational parameter. For each stage the total vacuum thrust T_0 and the total thrust inside the atmosphere T are related by

$$T = T_0 - P_a A_e \tag{27}$$

where P_a is the ambient atmospheric pressure and A_e the sum of the nozzle exit areas of the engines that are on. For each engine the nozzle exit area is 3.7515 m^2. The ambient pressure P_a and atmospheric density $\bar{\rho}$ are approximated by exponential functions of the altitude. The aerodynamic lift and drag forces are modeled by

$$L = \tfrac{1}{2}\bar{\rho}v^2 S_{\text{ref}} C_L, \qquad C_D = \tfrac{1}{2}\bar{\rho}v^2 S_{\text{ref}} C_D \tag{28}$$

with S_{ref} being the reference area of the vehicle. The lift and drag coefficients C_L and C_D of the vehicle are originally given in the form of tabulated data as functions of Mach number M and angle of attack $\alpha = \theta - \gamma$. In this study, C_L for the first stage is modeled by

$$C_L = C_{L1}(M)\alpha + C_{L2}(M)\alpha^2 \tag{29}$$

where C_{L1} and C_{L2} are the least-squares fittings to the tabulated data over α for a given Mach number M and then interpolated by cubic splines over M. The term C_D is fitted by

$$C_D = \begin{cases} C_{D0}(M) + C_{D2}(M)\alpha^2, & 0 \le M \le 2.5 \\ C_{D0}(M) + C_{D2}(M)(\alpha-\alpha_1)^2, & 2.5 < M \end{cases} \tag{30}$$

where $\alpha_1 = 10$ deg, and in each case C_{D0} and C_{D2} are similarly fitted by cubic splines as C_{L1} and C_{L2} are. These fittings match the table lookup of the tabulated data quite well. For the second stage, since the vehicle is already out of the dense atmosphere and $M > 8$, a constant $C_D = 0.22$ and $C_L = 0$ are used. This means zero lift and an approximate value for drag. For both stages, the control is the pitch angle θ.

For the given payload and inert masses, the trajectory optimization problem is to find the best mass ratios for the booster and the core vehicle, and the optimal control history $\theta^*(t)$ such that the minimum amount of fuel is required for the mission. This is equivalent to minimization of the mass at liftoff. The initial conditions for the optimal trajectory are set as

$$\begin{aligned} r(0) &= 6378.4 \text{ km (an altitude of 400 m)} \\ v(0) &= 65 \text{ m/s}, \qquad \gamma(0) = 89.5 \text{ deg} \end{aligned} \tag{31}$$

The initial mass $m(0)$ is to be minimized subject to the orbital insertion conditions

$$\begin{aligned} r(t_f) &= 6526.16 \text{ km}, \qquad v(t_f) = 7855.121 \text{ m/s} \\ \gamma(t_f) &= 0, \qquad m(t_f) = 152{,}052 \text{ kg} \end{aligned} \tag{32}$$

where the $m(t_f)$ is the sum of the masses of the payload, fairing, and inert mass of the core vehicle. The time of flight t_f is determined via the mass equation by the total amount of propellant used, which is in turn determined by the mass ratios. Other inequality constraints are

$$-4 \text{ deg} \le \alpha = \theta - \gamma \le 14 \text{ deg} \tag{33}$$

$$q \le 40698 \text{ (Pa)} \tag{34}$$

$$|\alpha q| \le 2925 \text{ (rad-Pa)} \tag{35}$$

where $q = 0.5\bar{\rho}v^2$ is the dynamic pressure. The constraint on α results from the fact that the aerodynamic data are given for α in that range. The trajectory optimization problem is converted into a nonlinear programming problem by parameterizing $\theta(t)$ by cubic splines functions of time. The nodes of the splines plus the two parameters that specify the masses of fuel of the booster and core vehicle constitute a parameter optimization problem. The state inequality constraints (34) and (35) are transformed into terminal constraints

$$w(t_f) \ge 0, \qquad z(t_f) \ge 0$$

where

$$\begin{aligned} \dot{w} &= \min(0,\ 40698 - q), \qquad w(0) = 0 \\ \dot{z} &= \min(0,\ 2925 - |\alpha q|), \qquad z(0) = 0 \end{aligned}$$

A global optimization method based on a continuous simulated annealing algorithm[19] was first used to produce a solution in the proximity of the optimal solution. This solution was in turn used as the initial point for a sequential quadratic programming algorithm[20] to locate accurately the optimal solution.

The optimal solution turned out to call for a full tank of fuel for the core vehicle and a 94.5% full tank for the booster. This translates into a liftoff mass of 1,573,835 kg, corresponding to a fuel saving of 34,926 kg as compared with nonoptimal trajectories that could easily use up all of the fuel the vehicle can carry for the same mission. The staging occurred 150 s after liftoff at an altitude of 61.6 km and velocity of 2.63 km/s. The complete flight lasted 370 s. Figure 3 shows the altitude profile along the optimal ascent trajectory. The inequality constraint (34) was not active, but constraint (35) was. Figure 4 shows the variation of αq during the flight.

Trajectory-Tracking Guidance Law

Now the task is to derive a feedback guidance law for $\theta(t)$ to track the optimal trajectory obtained. For better numerical conditioning, the following dimensionless variables are used:

$$\begin{aligned} \tau &= \frac{t}{\sqrt{r_0/g_0}}, \qquad Y = \frac{r}{r_0}, \qquad V = \frac{v}{\sqrt{g_0 r_0}} \\ A_T &= \frac{T}{mg_0}, \qquad A_D = \frac{D}{mg_0}, \qquad A_L = \frac{L}{mg_0} \end{aligned} \tag{36}$$

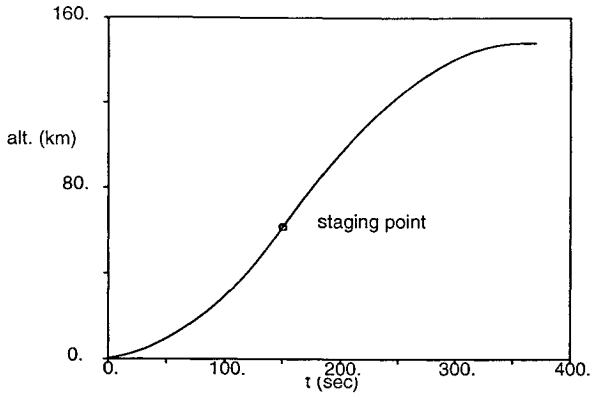

Fig. 3 Nominal ascent trajectory.

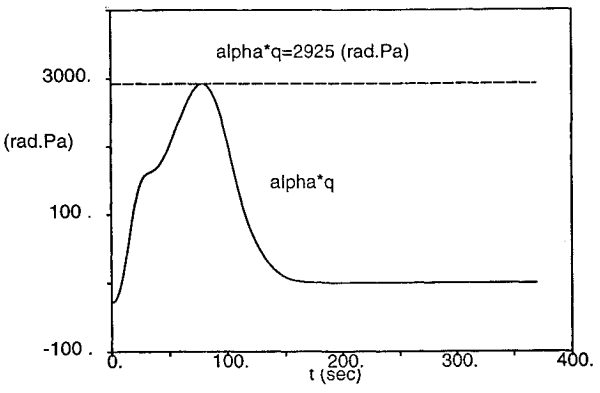

Fig. 4 Variation of αq history along the nominal trajectory.

where $r_0 = 6378$ km (radius of the Earth), and $g_0 = \mu/r_0$. In addition, we will use the climb rate $Z = \mathrm{d}Y/\mathrm{d}\tau = V\sin\gamma$ in place of the flight-path angle γ. This has two benefits: the feedback control law will be dependent on Z, which is easier to measure than γ, and the proof of asymptotic tracking convergence with the use of Z is straightforward. Thus, in the new dimensionless variables, the system equations are

$$Y' = Z \tag{37}$$

$$Z' = (V^2/Y) - (1/Y^2) - (Z^2/Y) + [A_T\cos(\theta-\gamma) - A_D] \times (Z/V) + [A_T\sin(\theta-\gamma) + A_L]\sqrt{1-(Z/V)^2} \tag{38}$$

$$V' = A_T\cos(\theta-\gamma) - A_D - (Z/VY^2) \tag{39}$$

where the prime stands for the differentiation with respect to τ. The mass equation is ignored because it simply determines a linear variation of $m(\tau)$. Note that both A_D and A_L depend on θ through α. Without throttling the rocket engines and with fixed burn times, feedback velocity regulation cannot be achieved effectively. Therefore we will only concentrate on the flight-path control, that is, Eqs. (37) and (38). If we define a new control as

$$u = [A_T\cos(\theta-\gamma) - A_D](Z/V) + [A_T\sin(\theta-\gamma) + A_L]\sqrt{1-(Z/V)^2} \tag{40}$$

and let $x_1 = Y$ and $x_2 = Z$, then the system (37) and (38) has the form of Eqs. (17) and (18) with $A = 1$. The corresponding $B_2 = 1$. Following Theorem 2, we conclude that u given by Eq. (19) will lead to globally asymptotically stable tracking of any feasible flight path specified by $[Y^*(t)\ Z^*(t)]$ for any $h > 0$, provided that no control saturation occurs. Particularly, if the weightings are chosen to be $Q_1 = Q_Y$, $Q_2 = Q_Z$, and $R = 0$, the closed-loop dynamics according to Eqs. (21) and (22) are

$$\Delta Y'' + \frac{1}{h}\frac{Q_Z + 0.5h^2Q_Y}{Q_Z + 0.25h^2Q_Y}\Delta Y' + \frac{Q_Y}{2Q_Z + 0.5h^2Q_Y}\Delta Y = 0 \tag{41}$$

which is clearly stable for any $Q_Y > 0$, $Q_Z > 0$, and $h > 0$. Also, if a desired damping ratio ξ for the closed-loop altitude dynamics is specified, it is easy to show from Eq. (41) that the required ratio of $\sigma = Q_Y/Q_Z$ is given by

$$\sigma = \frac{2}{h^2}\left(-1 + \frac{\xi\sqrt{4\xi^2-2}}{2\xi^2-1}\right) \tag{42}$$

Clearly, for σ to have a positive real solution, we must have $\xi \geq 1/\sqrt{2}$. With little effort we can show that $\sigma \to \infty$ when $\xi \to 1/\sqrt{2}$, and $\sigma \to 0$ when $\xi \to \infty$. Equation (42) provides a guideline for selecting the values of Q_Y and Q_V.

Despite the tracking convergence proof, the control law for u is not convenient to use because of two reasons: 1) once u is obtained from Eq. (19), the actual control θ still needs to be solved for iteratively from Eq. (40) (note that A_D and A_L depend on θ nonlinearly); and 2) the constraint $-4\,\text{deg} \leq \alpha \leq 14\,\text{deg}$ and the trajectory constraint (35) are not easy to enforce in terms of simple saturation on u. Therefore, we will implement the implicit version of the control law (14) instead. Again we stress that the control laws (11) and (14) achieve the same objective of minimizing the predicted tracking errors [Eq. (9)] as $R \to 0$.

Let $R > 0$ be specified. The guidance law by Eq. (14) for θ is

$$\theta(\tau) = s\Big(\theta^*(\tau) - hR^{-1}\Big\{0.5hQ_YG_{21} \times \big[\Delta Y + h\Delta Z + 0.5h^2\big(f_{22} + g_{22} - Z'^*\big)\big] + G_{21}Q_Z\big[\Delta Z + h\big(f_{22} + g_{22} - Z^{*\prime}\big)\big]\Big\}\Big) \tag{43}$$

where s is a saturation function defined in Eq. (13), and

$$f_{22} = (V^2/Y) - (1/Y^2) - (Z^2/Y)$$

$$g_{22} = [A_T\cos(\theta-\gamma) - A_D](Z/V) + [A_T\sin(\theta-\gamma) + A_L]\sqrt{1-(Z/V)^2}$$

$$G_{21} = -\left[A_T\sin(\theta-\gamma) + \frac{\partial A_D}{\partial\alpha}\right]\frac{Z}{V} + \left[A_T\cos(\theta-\gamma) + \frac{\partial A_L}{\partial\alpha}\right]\sqrt{1-\left(\frac{Z}{V}\right)^2}$$

where

$$\frac{\partial A_L}{\partial\alpha} = \frac{\bar{\rho}v^2S_{\text{ref}}}{2mg_0}\frac{\partial C_L}{\partial\alpha}, \qquad \frac{\partial A_D}{\partial\alpha} = \frac{\bar{\rho}v^2S_{\text{ref}}}{2mg_0}\frac{\partial C_D}{\partial\alpha}$$

For the second stage, $A_L = 0$ and A_D is calculated with $C_D = 0.22$.

The obvious function of the saturater s in Eq. (43) is to enforce the constraint

$$-4\,\text{deg} + \gamma \leq \theta \leq 14\,\text{deg} + \gamma \tag{44}$$

which is from $-4\,\text{deg} \leq \alpha \leq 14\,\text{deg}$. But for this launch vehicle, the satisfaction of the critical trajectory constraint (35), which is equivalent to

$$(-2925/q) + \gamma \leq \theta \leq (2925/q) + \gamma \tag{45}$$

must also be guaranteed in the presence of trajectory dispersions, because this constraint is already active along the nominal trajectory. The fact that the current approach permits the control constraints to be state dependent allows us to enforce both Eqs. (44) and (45) easily. In fact, we can combine the two requirements (44) and (45) by choosing the saturation bounds

$$U = \min\{14\,\text{deg} + \gamma,\ (2925/q) + \gamma\} \tag{46}$$

$$L = \max\{-4\,\text{deg} + \gamma,\ (-2925/q) + \gamma\} \tag{47}$$

in the definition of the saturater s. Then θ obtained from Eq. (43) guarantees the satisfaction of both constraints. For additional control rate constraints and other more general types of trajectory constraints, the same advantage of the current approach remains true, although a little more development is required.

Numerical Simulations

The performance of the guidance laws (43) was tested by creating some hypothetic off-nominal perturbations and disturbances. Before proceeding with simulation, we notice that the θ calculated from Eq. (43) may call for an initial $\theta(0)$ that is different from the actual pitch angle of the vehicle, depending on different initial conditions. Also, the rate of θ has no limits, which allows very fast changes and even discontinuities in θ. Therefore the simulated tracking performance can be overly optimistic, because these occurrences are not realistic, given that θ is a physical variable determined by the rotational dynamics of the vehicle. To compensate partially the system dynamics in responding to the θ command, we use a first-order lag

$$\dot{\theta} = \tfrac{1}{4}(-\theta + \theta_{\text{com}}) \tag{48}$$

with $\theta(0) = \gamma(0) = 89.5$ deg, where θ_{com} is the solutions of Eq. (43), and θ is the value used in simulation.

For numerical computation, the following parameters were chosen in the guidance law,

$$Q_Y = 200{,}000, \qquad Q_Z = 20, \qquad h = 0.1 \tag{49}$$

where the values of Q_Y and Q_Z correspond to $\xi = 0.7072$ by Eq. (42). The value of h is in nondimensional τ, which corresponds to a real time of 80.6 s, whereas the integration step size was 0.001 in τ with a standard Runge–Kutta fourth-order algorithm. This value of h that appears to give good tracking performance was determined through numerical simulations and was always first used when using the fixed-point iteration (15) to solve for θ_{com} from Eq. (43). The size of h was then halved if convergence (with an accuracy of 10^{-4}) had not been achieved within 30 iterations. This process continued until convergence occurred. The weighting R is selected to be

$$R(\tau) = 1.0 + (0.01 - 1.0)(\tau/\tau_f) \tag{50}$$

where τ_f is the total time of flight. This choice of decreasing R is found to enhance the tracking performance quite noticeably. It gives a relatively large R during the initial period when the tracking errors are large. This prevents the control from oversaturating. Once the tracking errors are reduced, R approaches small values to increase the tracking accuracy (recall that the asymptotic tracking requires $R \to 0$).

The first experiment was to test effectiveness of the guidance law in the event when the actual flight conditions are different from the nominal ones. Suppose that after the initial liftoff, the actual flight-path angle $\gamma(0)$ is 88 deg instead of the nominal 89.5 deg given in Eq. (31). This change of 1.5 deg for the kick angle would alter the ascent trajectory very dramatically if open-loop guidance is used for the first stage. But the feedback nature of the current guidance law enables it to adapt to the trajectory deviations. Plotted in Fig. 5 is the comparison of the nominal and guided altitude histories for $\Delta\gamma(0) = -1.5$ deg. The difference between the two trajectories is barely discernible. The orbital insertion errors along the guided trajectory are $\Delta r_f = 0.0028$ km, $\Delta v_f = -8.31$ m/s, and $\Delta\gamma_f = -0.027$ deg. Figure 6 contains the variations of the nominal and the guided pitch angle commands. If the launch vehicle, with $\Delta\gamma(0) = -1.5$ deg, is still guided by the nominal open-loop pitch angle command obtained in the trajectory optimization problem, the vehicle would crash into ground shortly after the burnout of the first stage, as shown also in Fig. 5 (marked as the unguided trajectory). In this case, even if the second stage employs a closed-loop guidance scheme, it is already too late to recover.

The typical number of the fixed-point iterations at a point was 2–4, although the numbers ranged from 1 to 28 for convergence. The reduction of the size of h occurred at several points. The smallest value of h required for convergence was 0.003125 in τ and the largest value used was 0.1 in τ as given. The tolerance for convergence is set at 10^{-4}. It should be pointed out that we found that for this problem the preceding simple adaptive adjustment of h resulted in much better tracking accuracy, rendering tracking errors at least an order of magnitude smaller as compared with the case where a small constant value for h (for instance, 0.003125) was used instead.

Table 1 Test for trajectory dispersions

Disturbances	Δr_f, km	Δv_f, m/s	$\Delta\gamma_f$, deg
$C_L = 0.7C_L^*$, $C_D = 1.3C_D^*$	0.060	−60.2	−0.054
$C_L = 1.3C_L^*$, $C_D = 0.7C_D^*$	−0.032	−48.9	−0.091
50% sinusoidal variations in $\bar{\rho}$ and P_a	0.043	−82.4	−0.064
Sinusoidal wind of 60 km/h	−0.045	−4.4	−0.074
Combined	−0.054	−155.3	−0.038
$T = 0.98T^*$, $I_{\text{sp}} = 0.98I_{\text{sp}}^*$	0.155	−212.7	−0.072

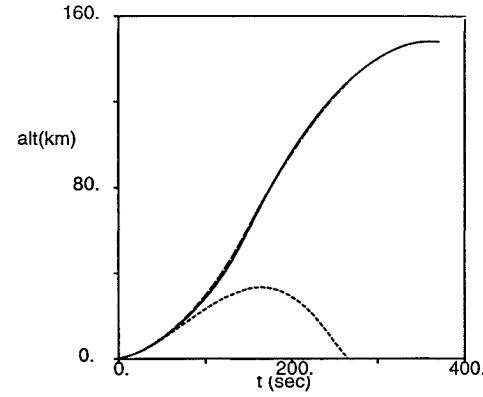

Fig. 5 Comparison of the altitude profiles for $\Delta\gamma_0 = -1.5$ deg: – – –, nominal; ——, guided; and - - - -, unguided.

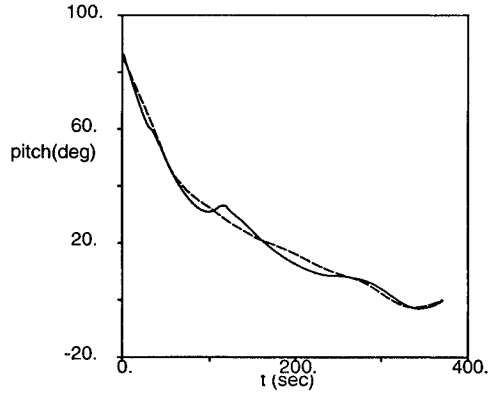

Fig. 6 Pitch angle $\theta(t)$ history for $\Delta\gamma_0 = -1.5$ deg: – – –, nominal; and ——, guided.

For a launch vehicle, the trajectory dispersions are largely caused by the inaccuracies in modeling of the launch system and disturbances in its surrounding environment. The basis on which the current guidance law is derived is continuous minimization of the errors between the predicted and nominal trajectories. This feature is expected to provide a certain degree of robustness. Table 1 summarizes the orbital insertion errors for some cases we tested for modeling uncertainties and external disturbances. The guidance algorithm only uses the nominal values of the perturbed parameters but assumes accurate full-state feedback. In particular, the dynamic pressure used in the guidance command calculation is assumed to be accurate, because this directly affects how accurate the trajectory constraint (35) can be enforced. The first two cases in Table 1 are for aerodynamic modeling uncertainties where the true lift coefficient is assumed to be 70%, and then 130% of the nominal value whereas C_D is assumed to be 30% higher, and then 30% lower than its nominal value. The third case considers

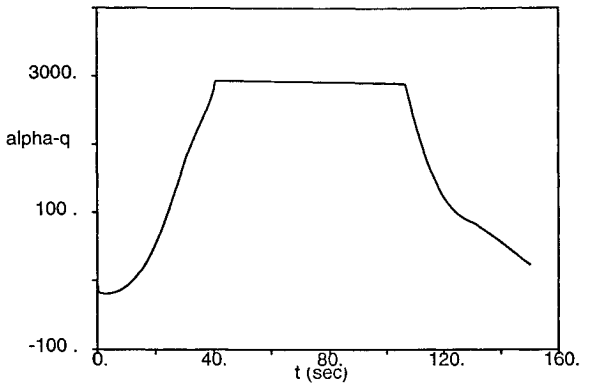

Fig. 7 Variation of αq (rad-Pa) in the presence of trajectory dispersions.

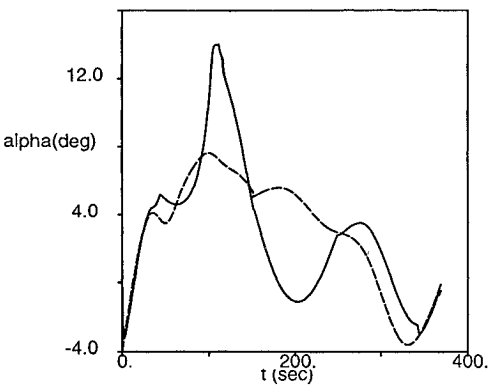

Fig. 8 Angle-of-attack history in the presence of trajectory dispersions: – – –, nominal; and ——, guided.

altitude-dependent variations of the atmospheric density $\bar{\rho}$ and pressure P_a of the form

$$\bar{\rho} = \bar{\rho}^* \left\{ 1 + 0.5 \sin \left[\frac{2\pi(r - R_0)}{50} \right] \right\}$$
$$P_a = P_a^* \left\{ 1 + 0.5 \sin \left[\frac{2\pi(r - R_0)}{50} \right] \right\} \tag{51}$$

where the quantities with an asterisk are the nominal ones. These variations affect the trajectory through the aerodynamic forces and magnitude of the thrust [Eq. (27)]. The wind tested in the fourth case is modeled as a horizontal tail-head wind with the speed of

$$W = -W_0 \cos[(r - R_0)\pi], \qquad 0 \le r - R_0 \le 10 \text{ km} \tag{52}$$

where $W_0 = 60$ km/h $= 12.5$ m/s, which is about 15 km/h higher than the maximum allowable wind speed at ground for launch of a Delta launch vehicle.[21] Note that in the presence of a wind the initial values of v (relative to the air) and γ are altered, as well as the dynamic equations for $\dot{v}$ and $\dot{\gamma}$. Again the guidance command generation is not informed of the wind perturbation. The combined case is when all of the disturbances in cases 1, 3, and 4 occur simultaneously. The last case assumes that the actual vacuum thrust and the specific impulse of the rocket engines are 2% lower than the nominal values.

The guidance law appears to cope with these common sources of trajectory dispersions quite well. It should be pointed out, though, that the primary effects of winds would be on the out-of-plane motion, which is not included in this study. There are no conceptual difficulties, however, to extend the current method to include lateral guidance. Also note that the velocity deviations are not actively regulated by the guidance law because the rocket engines are not throttleable. But the simulation results show that the velocity errors are bounded within a reasonable range. In certain cases, once the payload is delivered to the specified altitude with desired flight-path angle, firing of the rocket on board the payload may be necessary to increase the velocity to the desired level.

Figure 7 shows the variation of αq of the first stage along the guided trajectory in the combined case. The normal load constraint $|\alpha q| \le 2925$ (rad-Pa) is accurately satisfied by the guidance law, even in the presence of the considerable disturbances. The comparison of the nominal and guided α histories is depicted in Fig. 8. It can be seen that the constraint $-4 \text{ deg} \le \alpha \le 14$ deg is also strictly observed on the guided trajectory. This feature of enforcing control/trajectory constraints is a distinct advantage of the current method. It should be mentioned that the other trajectory constraint (34) is met by all of the trajectories [e.g., $q_{\max} = 35{,}000$ (Pa) in the combined case].

One important scenario that was not tested is the case where one engine fails. In such a case, tracking the nominal trajectory using the current guidance scheme probably is not a good strategy, since the vehicle would have some propellant left at the nominal staging or burnout time. Allowing the vehicle to continue the flight with some guidance compensation determined in preflight failure analysis may prove to be a better alternative.[16]

V. Conclusions

A systematic methodology is introduced for developing nonlinear guidance laws for aerospace vehicles with general nonlinear dynamics to track a prescribed nominal trajectory. The guidance laws are based on a nonlinear continuous predictive control approach. The guidance commands can be obtained reliably and efficiently using a fixed-point iteration algorithm that is guaranteed to converge when a guidance parameter is selected to be sufficiently small. Hard constraints on the trajectory are conveniently enforced by the guidance laws. The problem of guiding an advanced launch vehicle to track a predetermined trajectory is solved as an example. The tracking convergence is first established by transforming the system into one that is linearly dependent on the control, but the implementation uses the original complete nonlinear equations. It is demonstrated that the current guidance law, with appropriate choices of saturation bounds, enforces both angle-of-attack and a normal load constraints strictly while it produces accurate trajectory tracking in the presence of a variety of off-nominal launch conditions, modeling uncertainties, and environmental disturbances. This work suggests that the present guidance scheme may be ideal for other guidance problems, such as entry guidance of a reusable space vehicle, in which accurate trajectory tracking is desirable and various stringent trajectory constraints must be observed.

References

[1]Roenneke, A. J., and Markl, A., "Re-Entry Control of a Drag vs Energy Profile," *Journal of Guidance, Control, and Dynamics*, Vol. 17, No. 5, 1994, pp. 916–920.

[2]Isidori, A., *Nonlinear Control Systems: An Introduction*, 2nd ed., Springer–Verlag, New York, 1989.

[3]Meyer, G. R., Su, R., and Hunt, R. L., "Application of Nonlinear Transformations to Automatic Flight Control," *Automatica*, Vol. 20, No. 1, 1984, pp. 103–107.

[4]Lane, S. H., and Stengel, R. F., "Flight Control Design Using Nonlinear Inverse Dynamics," *Automatica*, Vol. 24, No. 4, 1988, pp. 471–483.

[5]Snell, S. A., Enns, D. F., and Garrard, W. L.,"Nonlinear Inversion Flight Control for a Supermaneuverable Aircraft," *Journal of Guidance, Control, and Dynamics*, Vol. 15, No. 4, 1992, pp. 976–984.

[6]Corban, J. E., Calise, A. J., and Flandro, G. A., "Rapid Near-Optimal Aerospace Plane Trajectory Generation and Guidance," *Journal of Guidance, Control, and Dynamics*, Vol. 14, No. 6, 1991, pp. 1181–1190.

[7]Van Buren, M. A., and Mease, K. D., "Aerospace Plane Guidance Using Time-Scale Decomposition and Feedback Linearization," *Journal of Guidance, Control, and Dynamics*, Vol. 15, No. 5, 1992, pp. 1166–1174.

[8]Powell, R. W., Shaughnessy, J. D., Cruz, C. I., and Naftel, J. C., "Ascent Performance of an Air-Breathing Horizontal-Takeoff Launch Vehicle," *Journal of Guidance, Control, and Dynamics*, Vol. 14, No. 4, 1991, pp. 834–839.

[9]Miele, A., Wang, T., and Melvin, W. W., "Guidance Strategies for Near-Optimum Take-Off Performance in a Windshear," *Journal of Optimization Theory and Applications*, Vol. 50, No. 1, 1986, pp. 1–47.

[10]Lu, P., "Trajectory Optimization and Guidance for an Advanced Launch Vehicle," AIAA Paper 92-0732, Jan. 1992.

[11]Lu, P., "Tracking Control of General Nonlinear Systems," *Proceedings of the 33rd IEEE Conference on Decision and Control*, Inst. of Electrical and Electronics Engineers, Vol. 4, Dec. 1994, pp. 3814, 3815.

[12]Lu, P., "Optimal Predictive Control of Continuous Nonlinear Systems," *International Journal of Control*, Vol. 62, No. 3, 1995, pp. 633–649.

[13]LaSalle, J., "Stability Theory for Ordinary Differential Equations," *Journal of Differential Equations*, Vol. 4, No. 1, 1968, pp. 57–65.

[14]Rao, P. P., "Titan IIIC Preflight and Postflight Trajectory Analysis," *Journal of Guidance, Control, and Dynamics*, Vol. 7, No. 2, 1984, pp. 161–166.

[15]McHenry, R. L., Brand, T. J., Long, A. D., Cockrell, B. F., and Thibodeau, J. R., "Space Shuttle Ascent Guidance, Navigation, and Control," *Journal of Astronautical Sciences*, Vol. 27, No. 1, 1979, pp. 1–38.

[16]Dhand, S. K., and Wong, K. K., "Robust Flight Design for an Advanced Launch System Vehicle," *Proceedings of the Guidance, Navigation, and Control Conference* (New Orleans, LA), Vol. 2, AIAA, Washington, DC, 1991, pp. 1059–1068.

[17]Feeley, T. S., and Speyer, J. L., "Techniques for Developing Approximate Optimal Advanced Launch System Guidance," *Journal of Guidance, Control, and Dynamics*, Vol. 17, No. 5, 1994, pp. 889–896.

[18]Leung, M. S. K., and Calise, A. J., "Hybrid Approach to Near-Optimal Launch Vehicle Guidance," *Journal of Guidance, Control, and Dynamics*, Vol. 17, No. 5, 1994, pp. 881–888.

[19]Lu, P., and Khan, M. A., "Nonsmooth Trajectory Optimization: An Approach Using Continuous Simulated Annealing," *Journal of Guidance, Control, and Dynamics*, Vol. 17, No. 4, 1994, pp. 685–691.

[20]Pouliot, M. R., "CONOPT2: A Rapidly Convergent Constrained Trajectory Optimization Program for TRAJEX," General Dynamics, Convair Div., Rept. GDC-SP-82-008, San Diego, CA, 1982.

[21]Anon., "Delta Launch Vehicle Secondary Payload Planner's Guide For NASA Missions," NASA Goddard Space Flight Center, Nov. 1993.